A Multi-Observatory Inter-Comparison of Line-of-Sight Synoptic Solar Magnetograms

P. Riley · M. Ben-Nun · J.A. Linker · Z. Mikic · L. Svalgaard · J. Harvey · L. Bertello · T. Hoeksema · Y. Liu · R. Ulrich

Abstract The observed photospheric magnetic field is a crucial parameter for understanding a range of fundamental solar and heliospheric phenomena. Synoptic maps, in particular, which are derived from the observed line-of-sight photospheric magnetic field and built

P. Riley (✉) · M. Ben-Nun · J.A. Linker · Z. Mikic
Predictive Science, 9990 Mesa Rim Road, Suite 170, San Diego, CA, USA
e-mail: pete@predsci.com

M. Ben-Nun
e-mail: mbennun@predsci.com

J.A. Linker
e-mail: linkerj@predsci.com

Z. Mikic
e-mail: mikicz@predsci.com

L. Svalgaard · T. Hoeksema · Y. Liu
Stanford University, Stanford, CA, USA

L. Svalgaard
e-mail: leif@leif.org

T. Hoeksema
e-mail: todd@solar2.stanford.edu

Y. Liu
e-mail: yliu@solar2.stanford.edu

J. Harvey · L. Bertello
NSO, Kitt Peak, Tucson, AZ, USA

J. Harvey
e-mail: jharvey@noao.edu

L. Bertello
e-mail: bertello@noao.edu

R. Ulrich
UCLA, Los Angeles, CA, USA
e-mail: ulrich@astro.ucla.edu

Ⓢ Springer

up over a period of 27 days, are the main driver for global numerical models of the solar corona and inner heliosphere. Yet, in spite of 60 years of measurements, quantitative estimates remain elusive. In this study, we compare maps from seven solar observatories (Stanford/WSO, NSO/KPVT, NSO/SOLIS, NSO/GONG, SOHO/MDI, UCLA/MWO, and SDO /HMI) to identify consistencies and differences among them. We find that while there is a general qualitative consensus, there are also some significant differences. We compute conversion factors that relate measurements made by one observatory to another using both synoptic map pixel-by-pixel and histogram-equating techniques, and we also estimate the correlation between datasets. For example, Wilcox Solar Observatory (WSO) synoptic maps must be multiplied by a factor of 3–4 to match Mount Wilson Observatory (MWO) estimates. Additionally, we find no evidence that the MWO saturation correction factor should be applied to WSO data, as has been done in previous studies. Finally, we explore the relationship between these datasets over more than a solar cycle, demonstrating that, with a few notable exceptions, the conversion factors remain relatively constant. While our study was able to quantitatively describe the relationship between the datasets, it did not uncover any obvious "ground truth." We offer several suggestions for how this may be addressed in the future.

Keywords Sun: Corona, evolution · Magnetic fields · Solar wind · Interplanetary medium · Potential field source surface model

1. Introduction

The Sun's photospheric, and by extension, coronal magnetic field is a crucial parameter that modulates a range of solar phenomena. The open, unsigned magnetic flux, *i.e.*, the component of the solar magnetic field that opens up into the heliosphere, in particular, is of fundamental scientific importance (*e.g.* Riley, 2007). For example, its long-term (on the time-scale of ≈ 100 years) changes undoubtedly affect the transport of cosmic rays (Lockwood, 2001). These long-term variations in cosmic ray fluxes, if present, may affect both technology and space, and even terrestrial climate (Bering *et al.*, 1998). Lockwood, Stamper, and Wild (1999) argued that the average open flux has risen by 40 % from 1964 to 1999 and, by correlation and then extrapolation using *aa* (a measure of the disturbance level of the Earth's magnetic field based on magnetometer observations at two approximately antipodal stations), by 131 % from 1900 to 1999. In contrast, Svalgaard and Cliver (2005) computed an index based on Bartel's historical *u* index of geomagnetic activity, and used it to infer that the average interplanetary magnetic field increased by only ≈ 25 % between 1900 and 1950, and has decreased since then. Most recently, Lockwood and Owens (2011) have suggested that the Sun, and by inference, its global heliospheric magnetic field, is entering a grand solar minimum period, potentially as deep as that thought to have occurred during the Maunder minimum.

An important aspect of these analyses concerns how raw solar magnetograms are processed to produce a line-of-sight, or radial estimates of the photospheric magnetic field in physical units.

Wang and Sheeley (1995), for example, have argued that a saturation correction factor derived for magnetograms at the Mount Wilson Observatory (MWO) should be applied to data measured at the Wilcox Solar Observatory (WSO). Their rationale was empirically based: it provided a significantly better match between the computed open flux (using a potential field source surface (PFSS) model) and the measured radial component of the

interplanetary magnetic field at 1 AU (B_r^{IMF}). Svalgaard, Duvall, and Scherrer (1978), in contrast, argued that WSO data require only a constant factor (1.85) to convert the measured values into units of gauss (G). Since these correction factors can, in places, differ by more than a factor of two, the choice of which one to use can be crucial.

A number of studies have attempted to inter-calibrate line-of-sight magnetograph measurements from one or more observatories (*e.g.* Jones, 1989, 1992a, 1992b; Jones *et al.*, 1993, 2004; Cauzzi *et al.*, 1993; Jones and Ceja, 2001; Berger and Lites, 2002; Thornton and Jones, 2002; Tran *et al.*, 2005; Wenzler *et al.*, 2006; Demidov *et al.*, 2008; Ulrich *et al.*, 2009; Pietarila *et al.*, 2013; Liu *et al.*, 2012). Typically, they were undertaken to resolve uncertainties in one dataset, under the assumption that the other data were more accurate. Our approach in this study, however, is to attempt to find a "ground truth" by comparing each of the seven observatories' data with every other observatory, in the hope that a consensus result may be found. Specifically, we analyze data from The Global Oscillation Network Group (GONG), Mount Wilson Observatory (MWO), Wilcox Solar Observatory (WSO), The Kitt Peak Vacuum Telescope (KPVT), Synoptic Optical Long-term Investigations of the Sun (SOLIS), the *Michelson Doppler Imager* (MDI) onboard the *Solar and Heliospheric Observatory* (SOHO) spacecraft (Scherrer *et al.*, 1995), and the *Helioseismic and Magnetic Imager* (HMI) onboard the *Solar Dynamics Observatory* (SDO) spacecraft. This combination was chosen because they represent the most often analyzed and used datasets, spanning and overlapping the greatest interval of time. Moreover, with the exception of KPVT, which was the predecessor of the SOLIS instrument, and MDI, which was retired recently, all of the observatories are currently producing synoptic maps.[1]

Unlike previous studies, we make the starting point for our analysis the synoptic maps, that is, latitude-longitude maps made up of 27 days of measurements, instead of the raw disk magnetograms. These are the maps that global numerical models rely on (Riley *et al.*, 2011; Bertello, Petrie, and Tran, 2010; Petrie, Canou, and Amari, 2011; Luhmann *et al.*, 2012) and thus represent an important basic dataset to investigate and assess. However, we must recognize that the process of making such maps, in and of itself, has the potential for introducing errors and even purposeful differences between the observatories. For example, our analysis will implicitly assume that the relationship between maps is a simple linear one, depending only on latitude, which is not likely to be the case.

Our goal in this study is limited to a quantitative comparison of the synoptic maps. Yet this in itself is a worthwhile objective. As Lord Kelvin wrote: "… when you can measure what you are speaking about, and express it in numbers, you know something about it; but when you cannot measure it, when you cannot express it in numbers, your knowledge is of a meager and unsatisfactory kind; it may be the beginning of knowledge, but you have scarcely in your thoughts advanced to the state of Science, whatever the matter may be." (Stellman, 1998). Here then, our study aims to place our current state of knowledge with respect to synoptic maps on Lord Kelvin's 'scale of science.' We first attempt to identify a "ground truth" for magnetic field values given in synoptic maps, and, failing that, to quantify the variability among them, which, at least to some extent, provides an estimate for their uncertainty.

---

[1]Since SOLIS replaced KPVT, we collectively refer to these data as "SOLIS" when we present long-term analyses, acknowledging that prior to Carrington rotation (CR) 2008, the data were obtained by KPVT.

2. Construction of Photospheric Synoptic Magnetograms

Magnetographs rely on a variety of techniques to infer the magnetic field in the photosphere. At MWO and WSO, for example, a Babcock solar magnetograph records the Zeeman polarization in the wings of an absorption line of iron at 5250 Å (*e.g.* Ulrich, 1992). Other lines are also measured to provide a true zero level of the instrument, such as the magnetically insensitive line of Fe I at 5124 Å at WSO.[2] By measuring the amount and sense of the circular polarization, the line-of-sight component of the magnetic field can be recovered. At NSO/KPVT, the 8688 Å line of Fe I is used to derive the LOS magnetic field (although 5507 Å was used for CR 1855 through 1862). Additionally, two distinct instruments were used: Between CR 1625 and CR1853, a 512-channel Babcock type instrument was used, while after CR 1855 a CCD spectromagnetograph was used. To convert the raw measurements into G, a conversion factor of 1.46 is required. Both MDI and GONG use interferometric techniques to measure the opposite states of polarization of the Ni I 6768 Å line.

Zeeman-splitting measurements must be carefully processed to infer the line-of-sight component of the photospheric magnetic field. Once obtained, assuming the field is vertical, a radial component can be derived. At MWO, two Fe I lines have been studied in detail: 5250 Å and 5233 Å. The former suffers from the problem that the magnetograph signal does not scale linearly with the line-of-sight component of the field, *i.e.*, it becomes saturated. Ulrich (1992) derived a correction factor for MWO 5250 Å observations of the form

$$g_{\mathrm{MWO}} = 4.5 - 2.5 \sin^2(\rho), \tag{1}$$

where ρ is the heliocentric angular distance away from disk center. Thus, multiplication of 5250 Å measurements by the factor given in Equation (1) would convert them to the 5233 Å measurements. This led Wang and Sheeley (1995) to apply the same correction factor to WSO data. However, Svalgaard, Duvall, and Scherrer (1978) found from their 5250 Å measurements at WSO that the line-of-sight photospheric field varied exactly as $\cos(\rho)$, and they inferred a constant saturation factor, $g_{\mathrm{WSO}} = 1.8$ (which has since been revised to 1.85 (Svalgaard, 2006)). The corrections for MWO and WSO measurements continue to be investigated. Recent work (Ulrich *et al.*, 2009; Demidov and Balthasar, 2009; Demidov and Balthasar, 2012) produced different and contradictory versions of Equation (1).

Beyond instrumental differences, we should note that the choice of wavelength itself necessarily means that we are not observing at the same height in the solar atmosphere. Thus, although the differences would be expected to be modest, strictly speaking, the instruments are not measuring exactly the same altitude in the solar atmosphere.

An additional practical difference is that the resolution of the disk magnetograms produced by different observatories (and even intra-observatory) varies dramatically. At the NSO KPVT, for example, the pixel size of images was 1.0″ for the 512-channel Babcock instrument and 1.14″ for the spectromagnetograph. Until 2010 SOLIS's resolution was 1.125″, becoming 1.0″ after that. Full-disk scan times have ranged from 40 min for the 512-channel Babcock instrument to 11 min for SOLIS. Ground-based observations, while in principle providing higher-resolution images, suffer from seeing effects that reduce the resolution to that of space-based instruments. The effective resolution of the disk magnetograms then defines the appropriate resolution at which synoptic maps can be made.

---

[2]Strictly speaking, the 5124 Å line does have a slight Zeeman sensitivity – $g = -0.013$ (Landi Degl'Innocenti, 1982).

Table 1 Sources of synoptic magnetograms used in this study: WSO data were obtained from wso.stanford.edu/synoptic/; GONG data were obtained from gong2.nso.edu/archive/patch.pl?menutype=s; Kitt Peak Vacuum Telescope (KPVT) data were obtained from nsokp.nso.edu/kpvt/synoptic/mag/; SOLIS data were obtained from solis.nso.edu/vsm/vsm_maps.php; MWO data were obtained from howard.astro.ucla.edu/pub/obs/synoptic_charts/FITS_files/; MDI data were obtained from soi.stanford.edu/magnetic/synoptic/carrot/M/; and HMI data were obtained from jsoc.stanford.edu/ajax/exportdata.html. For consistency, all data were downloaded on 1 October 2012, and analyzed thereafter.

Observatory	Type	Grid size	Dates available (mm/dd/year)	CRs available
WSO	LOS	73×30	05/27/1976 to 09/11/2012	1642 – 2127
GONG	Radial	360×180	08/25/2006 to 06/16/2010	2047 – 2097
KPVT	Radial	360×180	02/18/1975 to 09/26/2003	1625 – 2007
SOLIS	Radial	360×180[a]	08/30/2003 to 09/11/2012	2007 – 2127
MWO	LOS	971×512	06/28/1996 to 08/15/2012	1911 – 2126
MDI	Radial	3600×1080	05/05/1996 to 12/24/2010	1909 – 2104
HMI	Radial	3600×1440	04/22/2010 to 09/11/2012	2096 – 2127

[a]SOLIS maps are also available on 1800×900 grids.

Table 1 summarizes the main attributes of the synoptic maps we analyzed here. Column one gives the name of the observatory, while column two gives the type of measurement produced. In fact, all observatories measure only the line-of-sight component of the magnetic field; however, some convert this value into a "radial" field, under the assumption that the total field is radial, while others do not. Column three gives the grid size of the synoptic maps. These are the canonical values, although some of the observatories have special data products where the resolution may be different. Columns four and five give the dates and CRs over which the data are available.

Constructing synoptic maps, that is, maps of the radial photospheric magnetic field as a function of Carrington longitude versus latitude, can be a complex process. Some of the questions the observers must face in assembling them from disk images include the following: i) How is one to average data taken at different times during the day, or over multiple days, and, in the case of GONG, data from multiple observatories at different geographical locations? ii) How does one account for differential rotation for data taken at different times that were averaged together? iii) How does one fill in data in the polar regions, where because of geometrical effects one can observe not as well (or not at all) from Earth's vantage, due to the ± 7.2° tilt of the Earth's orbit with respect to the heliographic equatorial plane? For this study, our initial assumption in comparing the synoptic maps is that they have been processed in such a way as to reproduce the most accurate synoptic maps possible. However, we recognize that differences between them may reflect differences in how they are assembled, and not necessarily differences in the original data.

Unfortunately, synoptic maps themselves are not the best data product for driving MHD models. The name itself, synoptic, means "affording a general view of the whole," which suggests that the maps are a single snapshot in time; however, the maps are assembled using observations from near-Earth observatories taken during the course of a solar rotation, *i.e.*, at different times, and should, technically, be called diachronic maps. A more useful map for a global model would be a synchronic'(or true synoptic) map, that is, a snapshot of the entire solar surface at a single point in time. Such a map is not possible now or in the foreseeable future with our limited Earth-centric view of the Sun.

A step toward more synchronic maps can be made by accounting for the differential rotation that occurs as disk images are added to the synoptic map progressively farther around

the far-side of the Sun. Potential field source surface (PFSS) modeling suggests that these pseudo-synchronic maps, which include the effects of differential rotation, may produce better predictions of stream structure in the vicinity of Earth (Bertello, Petrie, and Tran, 2010). These results require further substantiation, however, and such maps are not produced as a matter of course by the other observatory teams, making them less than ideal for the present study. Flux evolution models arguably also provide a more accurate map of the photospheric magnetic field (Arge *et al.*, 2010). However, they remain very much a topic of research and are not yet regularly produced over a sufficiently long time span to be of use here.

Finally, we should note that some of the maps (but not all) have been re-processed over the years. The MDI data, for example, are currently (as of 1 October 2012) labeled LEVEL 1.8.2, reflecting a major re-processing of both the disk and synoptic products in December 2008. Unfortunately, time histories of previous versions are typically not made available, and we should emphasize that the results we derive here are sensitive to the version of the data analyzed. Thus, for clarity, all observatory data were downloaded on 1 October 2012, and the complete analysis described here was performed on those data.

3. Magnetogram Inter-Comparison

We begin our analysis by making some qualitative comparisons between the synoptic maps. We then turn to two quantitative approaches, linear regression and histogram equating, to estimate the relationship between flux measured at one observatory and another, before finally considering the possible temporal evolution of these relationships over more than a solar cycle.

Figure 1 summarizes all available synoptic maps as a function of longitude and $\sin(\lambda)$ from five solar observatories for CR 2047. These data have been plotted at their original resolution, that is, the resolution at which the maps were published, which can be quite different from the native resolution of the disk magnetograms. For example, the native resolution of WSO disk images is 23×11. Each map's color table was constructed by setting the range to be $\pm 5 \times |\tilde{x}|$, where $|\tilde{x}|$ is the median of the absolute value of each synoptic map. For the most part, the data are provided in self-describing FITS files that include the optional FSCALE or BSCALE keywords. For the WSO maps, which are supplied as text files, the data were converted from micro-tesla to gauss by multiplying by 0.01. The WSO data were neither corrected using the factor of 1.85, as advocated by Svalgaard (2006), nor using the MWO correction factor (Equation (1)), as proposed by Wang and Sheeley (1995). In the broadest sense then, the maps are reasonably similar to one another. The resolutions of these maps are 73×30 (WSO), 360×180 (GONG and SOLIS), 971×512 (MWO), and 3600×1080 (MDI). We note the ever-smaller scale features that appear with increasing resolution. The smallest-scale fields (outside active regions (ARs)) in the MWO are notable for their absence, when compared with SOLIS (panel above) or MDI (panel below). It is quite possible that these are not measured fields but noise in the data, which would be consistent with MWO's known low noise levels. On the other hand, the relative strength of the ARs at MWO is stronger (more saturated) than those for MDI. Thus, there is the suggestion that the fields do not scale linearly with strength between at least some of the observatories.

Figure 2 shows a second comparison for CR 2097, which occurred between 19 May 2010 and 16 June 2010. By this time, measurements of SDO's HMI were available. We note, again, the strong qualitative similarity between the magnetograms. WSO fields appear generally weaker, but we must bear in mind that the resolution of these data are at least a factor of five lower than the next-lowest resolved datasets, and some 50 times lower than
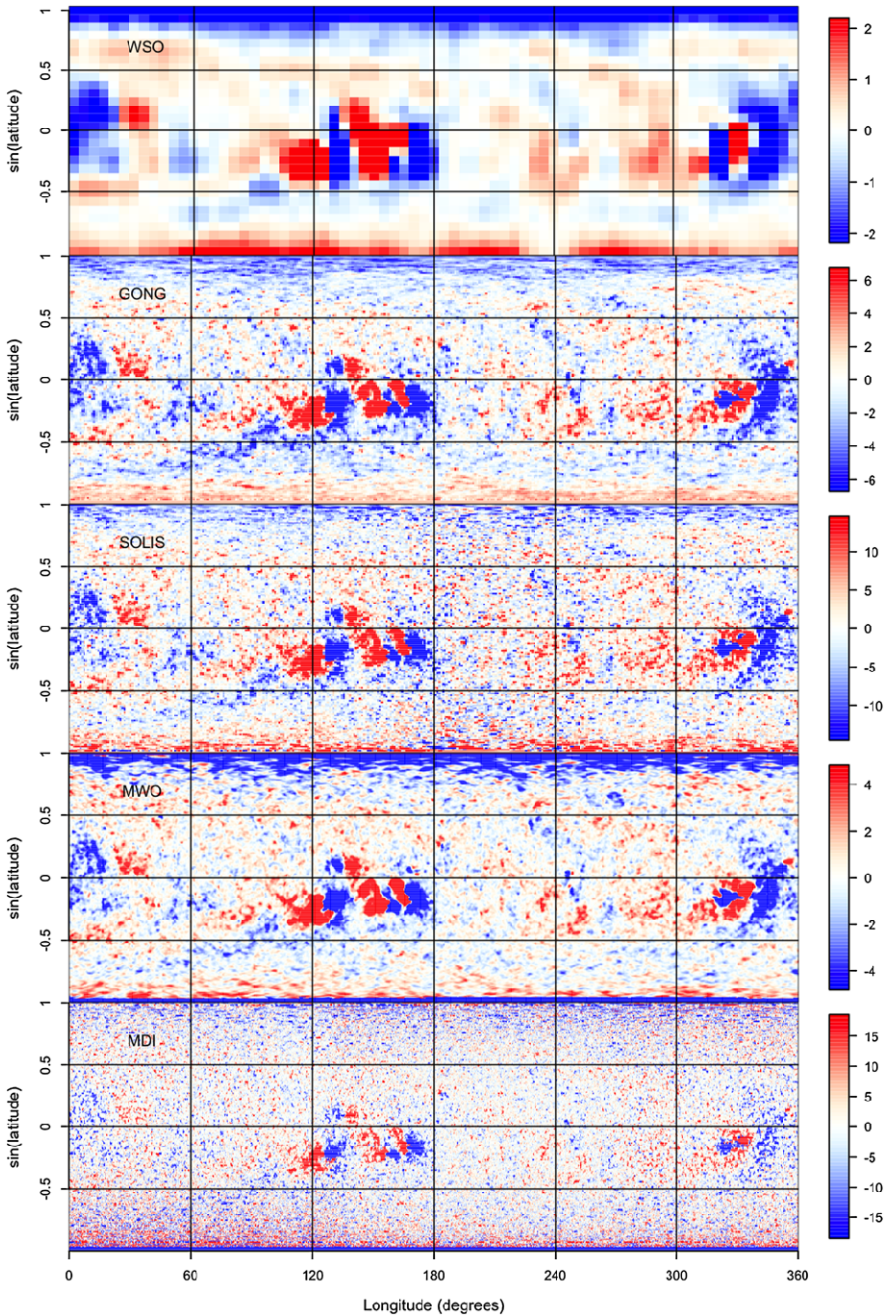
Figure 1 Comparison of synoptic maps (as a function of longitude and $\sin(\lambda)$) for five solar observatories for CR 2047. From top to bottom: Wilcox Solar Observatory (WSO); Global Oscillation Network Group (GONG); Synoptic Optical Long-term Investigations of the Sun (SOLIS), Mount Wilson Observatory (MWO); and *Michelson Doppler Imager* (MDI). All data are in their original resolution: WSO 73×30; GONG 360×180; SOLIS 360×180; MWO 971×512; and MDI 3600×1080. The ranges for the color bars were set to $\pm 5 \times |\tilde{x}|$, where $|\tilde{x}|$ is the median of the absolute value of each synoptic map.
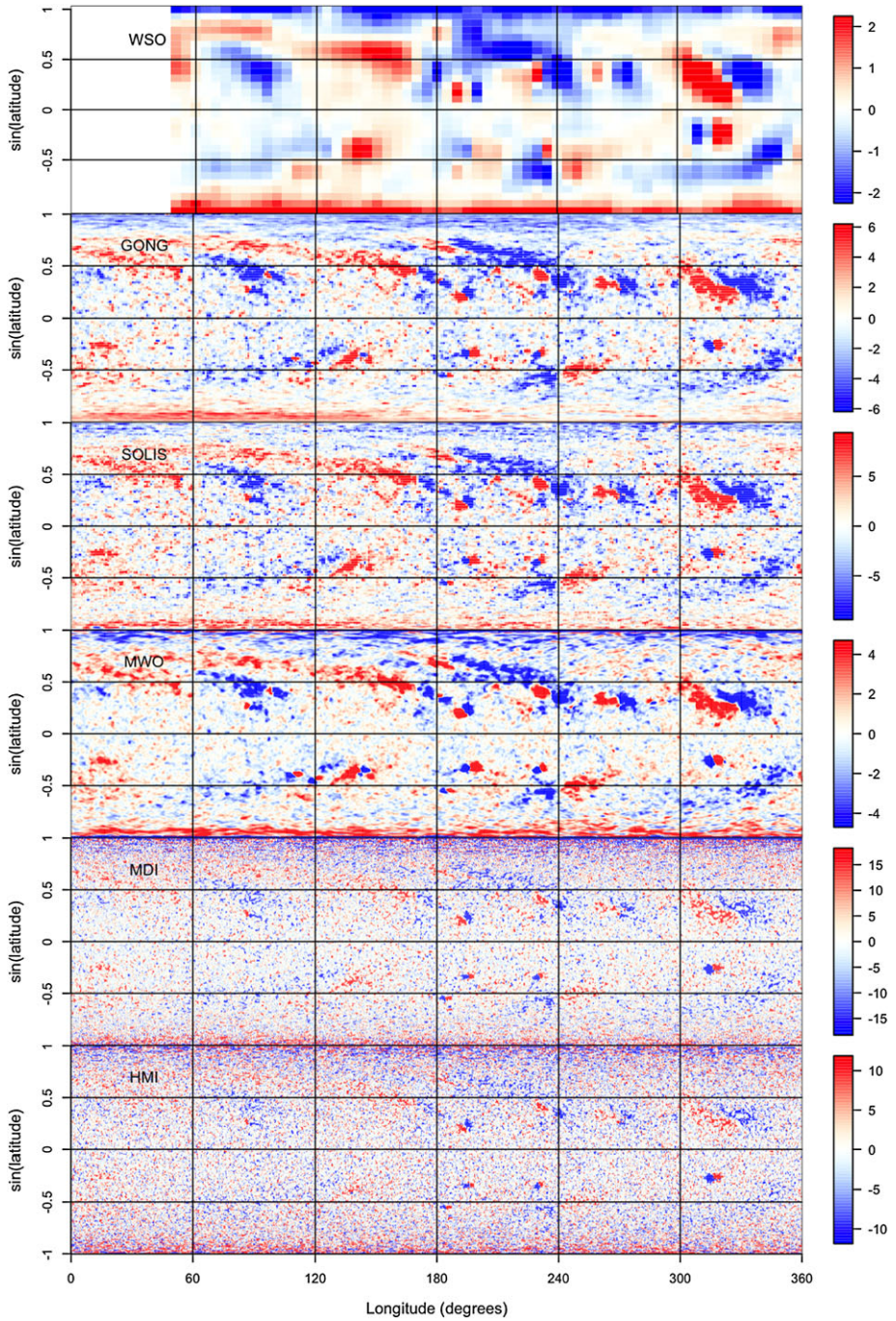
Figure 2 The same as Figure 1, except for CR 2097, which was also observed by SDO's HMI, with a resolution of 3600 × 1800.

HMI. MWO/MDI and GONG/SOLIS match well in terms of AR-scale fields, while the small-scale salt-and-pepper fields in the ten-times more resolved MDI and HMI are very similar, at least in a statistical sense.

In Figure 3 we have box-car-smoothed the data from GONG, SOLIS, MWO, and MDI for CR 2047 to match the resolution at WSO. In principle, these maps should match very closely, and, to a first appearance, they do. The AR structure at all observatories except WSO is remarkably similar, with the notable exception that the fields are weaker at MWO. Additionally, the quiet-Sun regions of MWO are weaker than at the other four observatories. Unfortunately, the smoothing procedure did not have the anticipated effect of converting the maps into WSO-proxies: The fields at WSO are still generally weaker than at other observatories. Also, more finer-scale structure is retained at the other observatories than at WSO. Although the data were smoothed on spatial scales matching WSO, they are still plotted at their native resolution, and so, in some sense, they still retain more information than does WSO.

4. Regression Analysis

To make a quantitative comparison of the synoptic maps, we constructed scatter plots and applied a selection of regression-fitting techniques to estimate the slope of the lines, which, in turn, gives us a measure of the conversion factor, that is, the coefficient necessary to take data from one observatory and convert them into data from another observatory. We also separated the data by $\sin(\lambda)$ bins for several reasons. First, the data become noisier with increasing distance from the equator to the poles. Thus, we can estimate the quality of the fits to the data by monitoring quantities such as correlation coefficients as a function of latitude. Second, it allows us to investigate whether there are any underlying latitudinal dependencies in the conversion factors, as has been proposed, for example by Wang and Sheeley (1995), for WSO data.

We begin by comparing data from GONG and MWO for CR 2047. Figure 4 shows scatterplots of the field at GONG (x-axis) and MWO (y-axis) as a function of $\sin(\lambda)$. From the top-left to the bottom-right panel, $\sin(\lambda)$ runs from -1 ($-90°$) to $+1$ ($+90°$). Focusing first on the low- and mid-latitude regions (middle panels) we note that i) the correlation is high (> 0.96), ii) the relationship is linear, and iii) the slopes of the best-fit lines are all close to 1.9. We also found that particularly when the scatter is large, it is useful to compute several estimates of the slope: In cases where they differ significantly (top and bottom rows), caution is appropriate in deciding whether the results are robust. Moving progressively closer to the poles, the correlation breaks down, such that by $|\sin(\lambda)| > 0.6$, the correlation coefficient has decreased significantly (< 0.5).

5. Histogram Equating

The technique of histogram equating was first applied to magnetogram comparisons by Jones *et al.* (1992). These authors found that pixel-by-pixel comparisons, such as those in Section 4, are complicated and prone to either intrinsic errors such as the timing of the measurements, or processing errors, such as filtering to account for the differences in spatial resolution of the instruments. A simpler approach, they argued, is to assume that the two instruments only observed the same statistical distribution of flux. Therefore, the only difference between cumulative histograms of two magnetograms is due to different scales
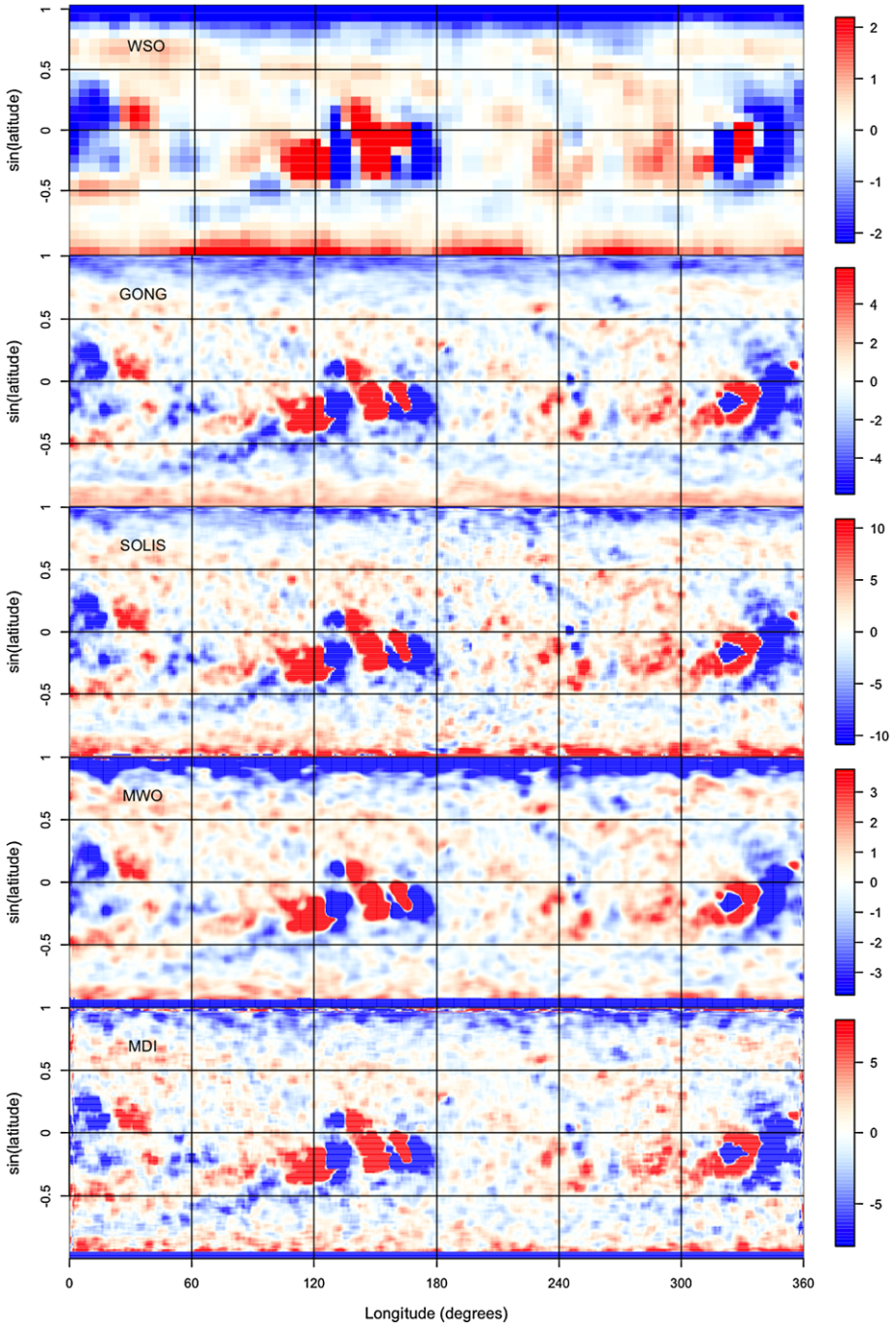
Figure 3 The same as Figure 1 (*i.e.*, for CR 2047), but the individual magnetograms have been box-car smoothed in both sin(λ) and longitude by the ratio of their resolution to that of WSO.
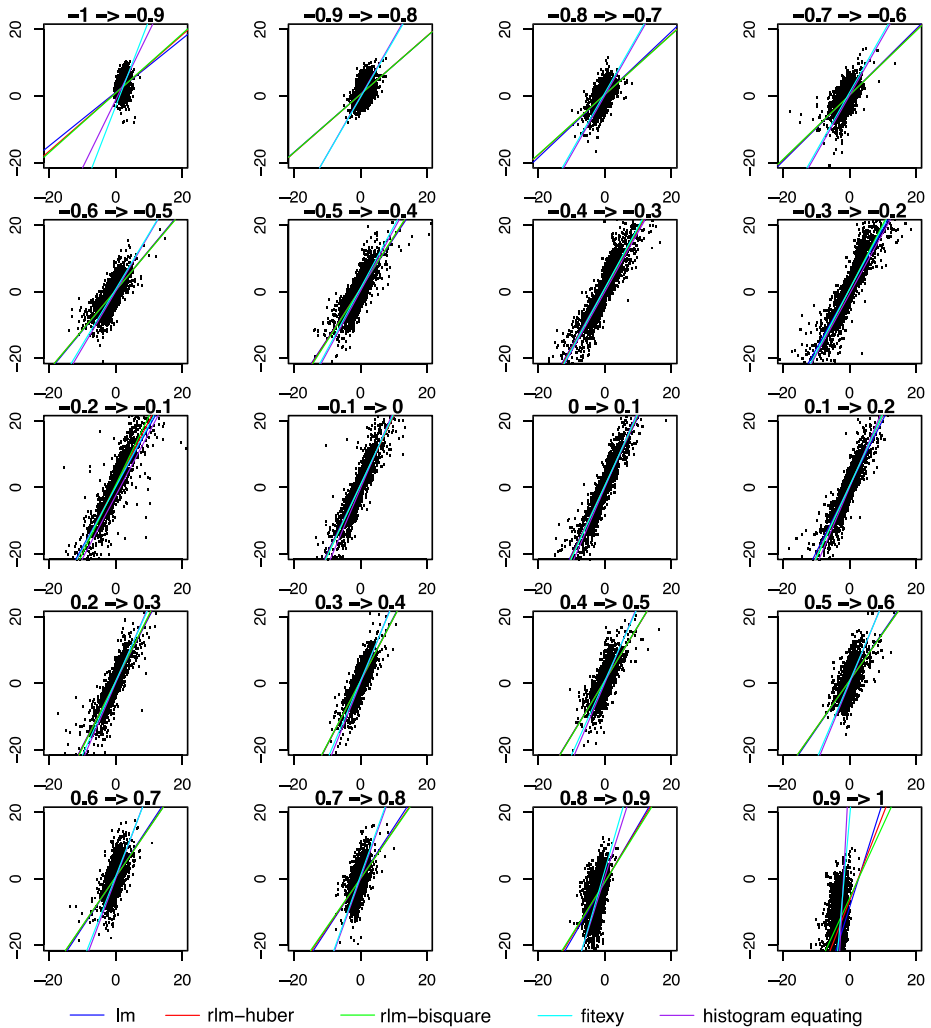
Figure 4 Correlation analysis for GONG (*x*-axis) and MWO (*y*-axis) for CR 2047 as a function of sin(λ). The panels start at $-90°$ (top left) and end with $+90°$ (bottom right) in equidistant steps of 0.1, in sin(λ). Both the *x*- and *y*-axes range from -20 Gauss to $+20$ Gauss. In each panel five straight lines are fitted to the data: blue – linear regression, red – robust linear regression with Huber weights, green – robust linear regression with bi-square weights, cyan – fitexy and purple – histogram equating (see text for more details).

of measurement. Additionally, this technique allows one in principle to identify conversion factors that are a function of flux. In practice, however, it should be noted that histogram equating must be used with care, and, in particular, the technique is quite sensitive to spatial resolution. In comparisons of GONG magnetograms, for example, it was found that 10-min averaged magnetograms taken at different times of day (but at the same GONG site) displayed diurnal variations that tracked seeing.

Here, we follow the technique explicitly outlined by Wenzler *et al.* (2006). Briefly, we first separated and ordered each of the n_{points} measurements into either positive or negative flux. We defined n_{bins} to be the number of bins ($= 100$ for comparisons not involving WSO,
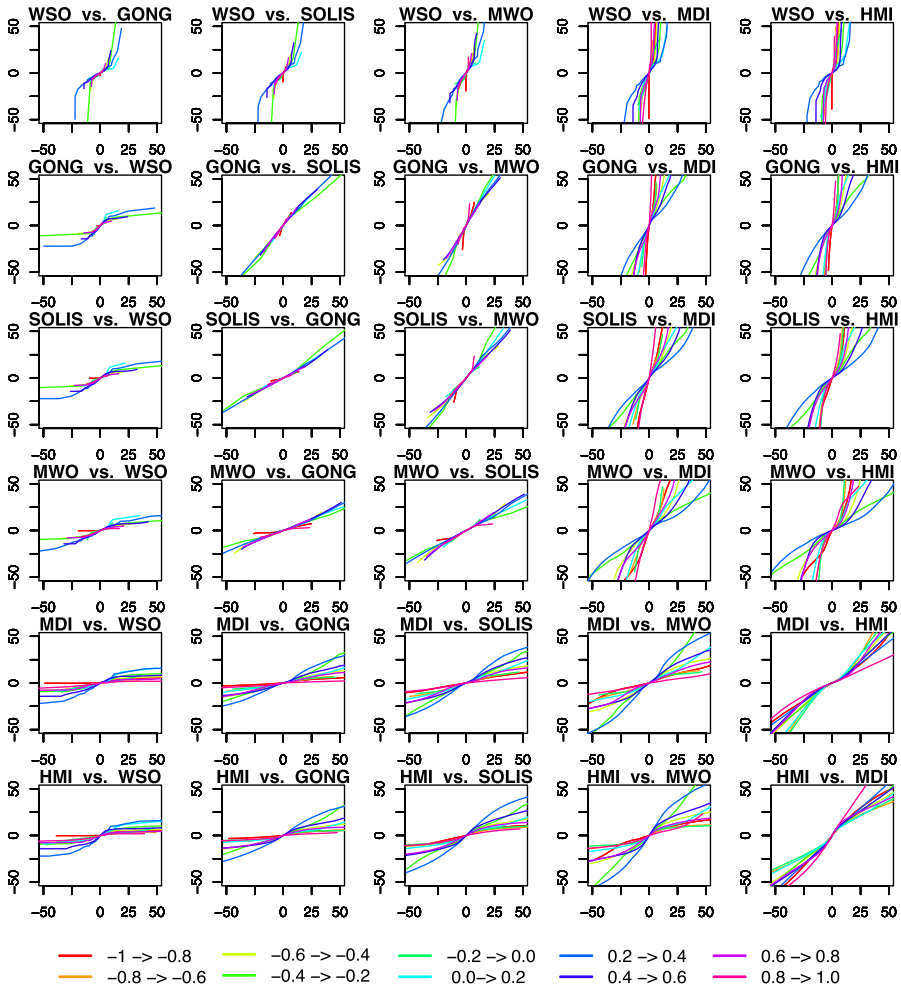
Figure 5 Comparison of histogram-equating tables for six observatories: WSO, GONG, SOLIS, MWO, MDI, and HMI for CR 2097. The leading diagonal comparison that would compare the same observatory with itself has been removed. The different-colored lines show comparisons for the bands in sin(λ) as indicated by the key at the bottom. All field strengths are in gauss.

and 50 if WSO is used) that each half of the measurements are apportioned, then sequentially grouped $\approx n_{points}/(2 \times n_{bins})$ into each bin. For each bin, we computed the mean field value. This then led to the so-called histogram-equating tables. Plots of these equating tables from one observatory against another one relate the strength of the field at one observatory to the strength at another observatory as a function of that flux.

Figure 5 compares histogram equating tables between the six observatories for CR 2097. In each panel, the different curves represent bands in sin(λ). The green to blue curves, for example, show the relationship between the fields within the vicinity of the solar equator, and are presumably the most accurate. We note several points. First, where the lines are straight, the conversion factor between the strengths of fields at one observatory and the other is independent of the strength of the flux. This can be seen in the MWO *vs.* SOLIS

comparisons. Similarly, where the curves have a strong S shape, there is a significant dependency on the conversion factor as a function of field strength, *i.e.*, a saturation effect. There are many examples of this, including MWO *vs.* HMI and WSO *vs.* GONG. The S shape may be regular, in which case for that comparison the field from the observatory along the y-axis saturates when the x-axis field reaches a certain value. Alternatively, the curve may be inverted, in which case the observatory plotted along the x-axis saturates with sufficiently strong field strengths from the y-axis observatory. It makes sense, intuitively, that the complementary plot (*i.e.*, observatory A *vs.* observatory B and observatory B *vs.* observatory A) will have regular and inverted shapes (see, *e.g.*, WSO *vs.* HMI and HMI *vs.* WSO). We note also that there is a strong symmetry between the positive and negative sides of each curve. Finally, we emphasize that in these comparisons we are limiting ourselves to the bulk measurements, which for the most part fall within the range of $-50 \rightarrow +50$ G. We believe that the deformities giving rise to the S shape are produced from sunspots, which are not likely to obey the same relationships as the lower-intensity fields from quiet-Sun and coronal-hole regions.

While the previous comparison highlighted the effects of $\sin(\lambda)$, in Figure 6 we compare equating tables for the five observatories that were contemporaneously taking measurements between CR 2047 and 2097. Thus, we are exploring the temporal variability of these curves. For each panel, we only retained data that fell within ± 0.5 in $\sin(\lambda)$, discarding polar values, which have the lowest signal-to-noise ratios. The slope and shape of the curves here should again give us a measure of the relationship between each pair of observatories, but now, the spread or variance in the curves within each panel gives us a measure of change over time. This may represent intrinsic random errors, and hence a measure of the limitations of such an approach, or may hint at systematic variations during the course of a solar cycle, which could, in principle, be incorporated into the conversion factor. A few points are in order. First, some comparisons result in straight, tightly grouped curves, such as those between SOLIS, GONG, and MWO. Comparisons involving either WSO or MDI lead to stronger S-shaped profiles. Moreover, this dependence with flux strength does not disappear when WSO and MDI are compared directly. Second, and this also relates to Figure 5, where a tightly grouped set of straight lines exists, a single conversion factor is defensible. However, where the profile is S-shaped and the lines are spread out, caveats of using a single conversion factor become significant.

6. Conversion Factors: Comparison of Techniques and Temporal Variations

In this section, we compare the linear regression and histogram-equating techniques for estimating the conversion factors, estimate their accuracy, and assess to what extent they vary over time.

Figure 7 summarizes the conversion factors for all combinations of the six observatories for CR 2097, obtained using the synoptic map pixel-by-pixel and histogram-equating techniques, and plotted as a function of $\sin(\lambda)$. Each panel shows the factor necessary to convert the data into one of the five other observatories. Thus, the middle-right panel, for example, shows that MWO data must be multiplied by a factor ≈ 5 for it to match the MDI measurements. (A subset of these data is summarized numerically in Tables 2 and 3.) We note several points. First, there seems to be little obvious trend with latitude: Although there is significant variability, the curves are, to a first approximation, flat. In particular, the WSO slopes show no evidence for a conversion factor proportional to $\sin^2(\lambda)$, which we would
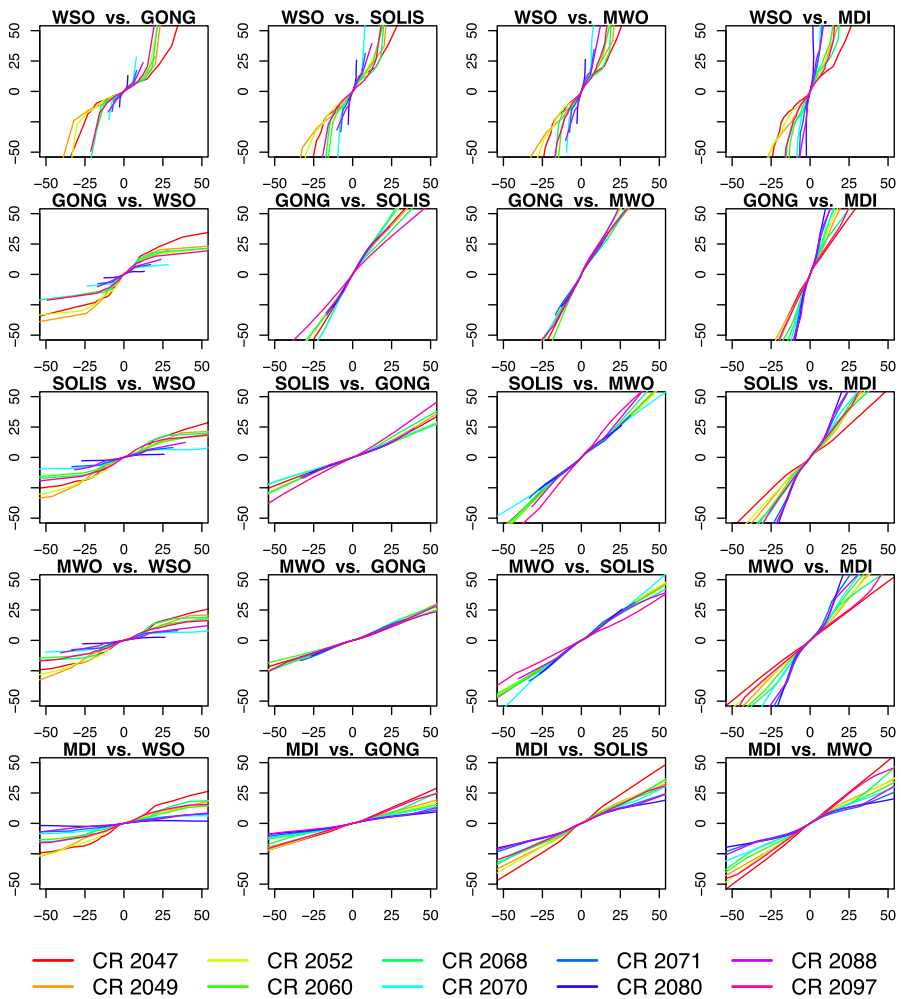
Figure 6 The same as Figure 5, but here, the different-colored lines show results for a selection of Carrington rotations from CR 2047 to CR 2097, as indicated by the key at the bottom.

anticipate if Equation (1) held for WSO data. Second, although often similar, the two techniques (pixel-by-pixel and histogram equating) show some significant differences. This is most apparent at high latitudes, where the data are the noisiest.

In Figure 8, we assess the accuracy of the slopes shown in Figure 7 via Pearson correlation coefficients (χ). As expected, the correlation for both the synoptic map pixel-by-pixel and histogram-equating techniques is best at low- and mid-latitudes and falls beyond $|\sin(\lambda)| = 0.5$. Generally speaking, the correlations for the histogram-equating technique are consistently better than for the pixel-by-pixel comparisons. Additionally, we note that the histogram-equating correlations are lowest where the histogram-equating tables (Figures 5 and 6) display the most nonlinear response (*i.e.*, S-shaped curve), such as between WSO and MDI or HMI and WSO.
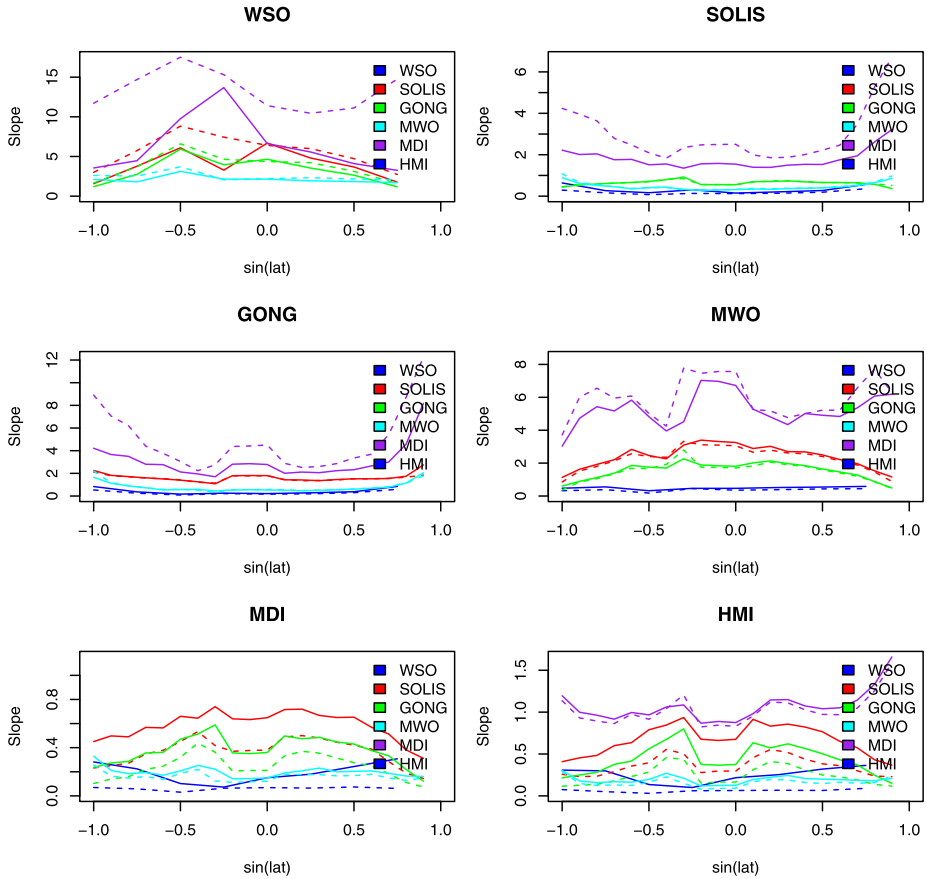
Figure 7 Conversion factors (slopes of pixel-by-pixel comparison, or linear regression of histogram equation tables) for six observatories compared against each other and plotted as a function of $\sin(\lambda)$. The solid line in each panel represents the pixel-by-pixel comparison while the dashed line represents the histogram-equating technique. Each observatory is assigned a different color. Each panel shows the factor necessary to convert the data into one of the five other observatories. Thus, the middle-right panel, for example, shows that MWO data must be multiplied by a factor ≈ 5 for it to match the MDI measurements. (See also Tables 2 and 3.)

To assess the variability of the conversion factors over time, we repeated the analysis previously described for CR 2097 for a selection of Carrington rotations spanning CR 1913 to CR 2127. We retained only data for which $|\sin(\lambda)| < 0.5$. Figure 9 summarizes these results. The curves start and stop at different times, depending on when the particular observatory was collecting data. Thus, GONG (top right) and HMI (bottom right), which only began taking measurements for CR 2047 and CR 2096, respectively, show the shortest traces. In contrast, WSO, SOLIS (made up of KPVT and SOLIS), and MWO show the longest traces because they have effectively been taking continuous measurements for $35-40$ years. As a first approximation, we might conclude that the profiles are relatively flat, suggesting no obvious temporal evolution in the conversion factor. That is, there is no obvious trend, which might occur if an instrument response function changed during this interval, or periodicity, which might occur if the conversion factors were sensitive to the solar cycle. That is not to
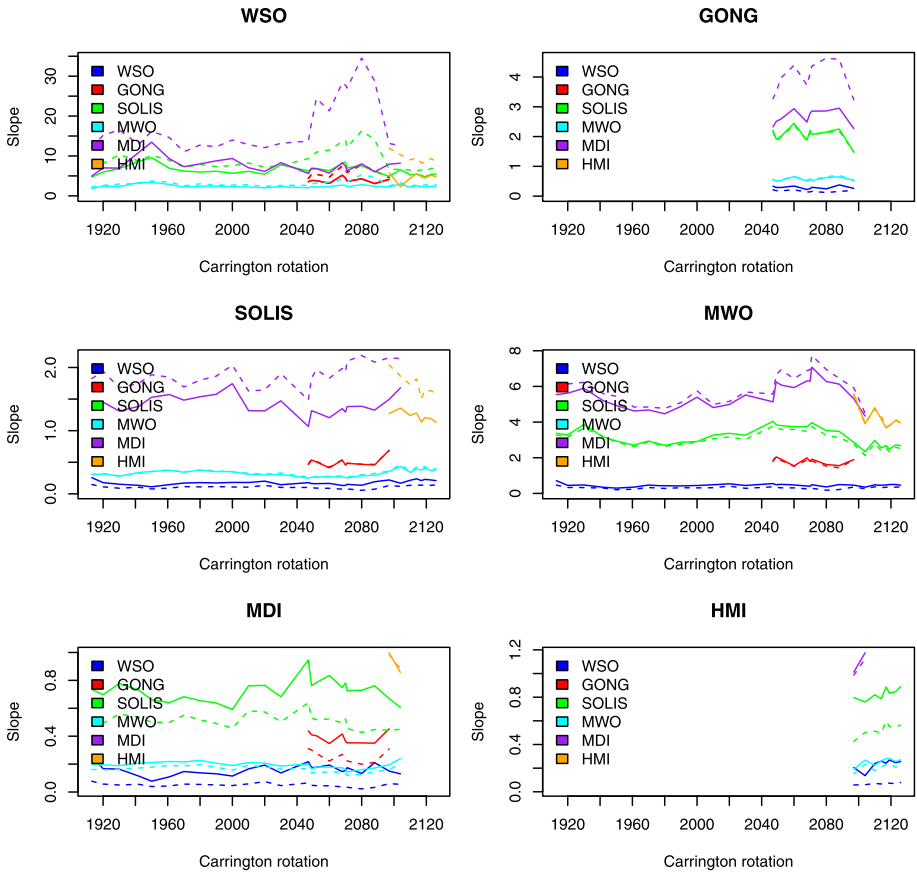
Carrington Rotation: 2097
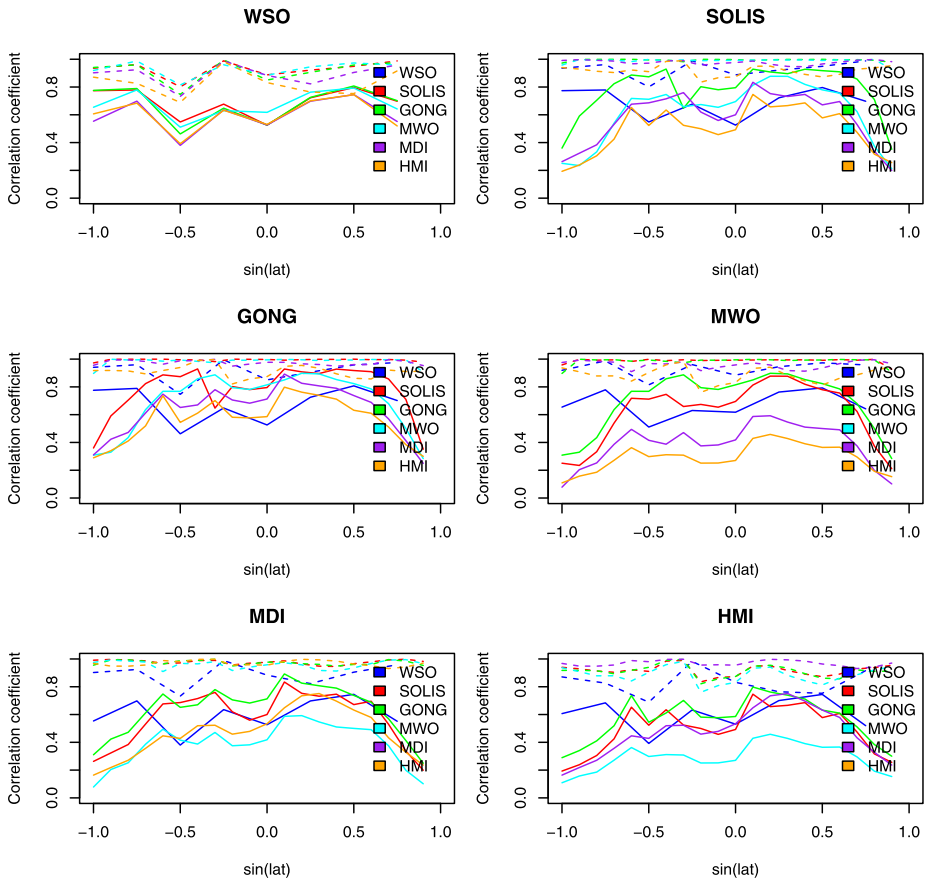
Figure 8 The same as Figure 7, except that correlation coefficients for CR 2097 are plotted as a function of sin(λ).

say that such variations are not present, only that they are not easily discerned. There are, however, some noteworthy points. First, the sharp rise (by a factor of ≈ 2.6) in the WSO-to-MDI conversion factor (top left panel). This started at ≈ CR 2050 and appears to have ceased before CR 2090. It should be noted, however, that this effect is amplified because of the already high conversion factor (≈ 12.5). Viewed as a reciprocal (bottom-left panel), the effect is not even noticeable. Since all traces in the WSO panel show this excursion, we infer that this is likely an artifact in the WSO dataset during this period. Second, the replacement of KPVT by SOLIS appears to be relatively seamless. The transition occurred around CR 2008, and while there is a drop in conversion factor (*e.g.*, middle-left panel), there is no systematic change to any of the profiles. Third, MDI and HMI, similarly dovetail nicely into one another (*e.g.*, middle-right panel). This is perhaps not surprising since the two datasets are produced by the same team at Stanford and the method for processing the original magnetograms is the same.

Tables 2 and 3 summarize numerically some of the results displayed in Figures 5 through 9. In Table 2, for example, we can see that WSO data must be multiplied by a

Figure 9 The same as Figure 7, except that the conversion factors are plotted as a function of Carrington rotation covering CR 1913 to CR 2127.

factor of $\approx 2 - 2.7$ to match data from MWO. This is close to the factor of 1.85 that Svalgaard (2006) has long advocated using for WSO data. Similarly, GONG must be multiplied by a factor of ≈ 2.2 to match data at SOLIS. This is consistent, although a little higher than the known deficit between GONG and SOLIS measurements.

Table 3 provides conversion factors for MWO as a function of Carrington rotation, that is, the factor that MWO measurements must be multiplied by for them to match data at the other observatory. Thus, MWO data must be multiplied by $1/3 - 1/2$ to match WSO observations, which is consistent with the values from Table 2.

From all of these comparisons, we conclude several points. First, there is no obvious "ground truth." That is, no two observatories consistently produce conversion factors of 1.0. There are pairs that have been made to match (KPVT/SOLIS and MDI/HMI), but no independent pairs. Second, the conversion factors are substantial, ranging up to an order of magnitude. Third, even for specific pair-wise comparisons, the conversion factor varies substantially over the course of a solar cycle.

Table 2 Inferred conversion factors for CR 2097. In each entry the first (second) number gives the slope from the pixel-by-pixel (histogram-equating) comparison, that is, reading down and to the left, this is the number you would need to multiply data from observatory 1 such that it matched data from observatory 2.

	WSO	GONG	SOLIS	MWO	MDI	HMI
WSO	1.0/1.0	$4.14 \pm 1.24/4.59 \pm 1.26$	$4.91 \pm 1.48/6.68 \pm 1.54$	$2.24 \pm 0.51/2.49 \pm 0.68$	$7.95 \pm 3.82/13.16 \pm 3.09$	$5.81 \pm 2.84/11.91 \pm 3.52$
GONG	$0.26 \pm 0.08/0.19 \pm 0.08$	1.0/1.0	$1.48 \pm 0.24/1.48 \pm 0.22$	$0.53 \pm 0.05/0.53 \pm 0.08$	$2.27 \pm 0.39/3.23 \pm 0.82$	$1.93 \pm 0.52/3.08 \pm 0.96$
SOLIS	$0.22 \pm 0.07/0.13 \pm 0.04$	$0.69 \pm 0.11/0.69 \pm 0.10$	1.0/1.0	$0.35 \pm 0.05/0.36 \pm 0.04$	$1.50 \pm 0.08/2.15 \pm 0.27$	$1.27 \pm 0.16/2.04 \pm 0.35$
MWO	$0.46 \pm 0.09/0.36 \pm 0.11$	$1.90 \pm 0.19/1.89 \pm 0.33$	$2.87 \pm 0.38/2.76 \pm 0.34$	1.0/1.0	$5.31 \pm 1.09/5.92 \pm 1.36$	$5.8 \pm 1.69/5.49 \pm 1.38$
MDI	$0.15 \pm 0.07/0.06 \pm 0.02$	$0.45 \pm 0.07/0.31 \pm 0.08$	$0.67 \pm 0.04/0.44 \pm 0.05$	$0.20 \pm 0.04/0.16 \pm 0.03$	1.0/1.0	$1.0 \pm 0.10/0.98 \pm 0.10$
HMI	$0.21 \pm 0.09/0.06 \pm 0.02$	$0.55 \pm 0.14/0.30 \pm 0.11$	$0.80 \pm 0.09/0.42 \pm 0.10$	$0.19 \pm 0.05/0.15 \pm 0.05$	$1.01 \pm 0.10/0.99 \pm 0.13$	1.0/1.0

Table 3 Inferred conversion factors and their standard deviations for a range of Carrington rotations from 1913 through 2126. The values have been scaled to MWO, so that MWO data from CR 1913 must be multiplied by 0.46 to match the values observed at WSO at this time. Where no data are available, dashes are present.

CR	WSO	GONG	KPVT	SOLIS	MWO	MDI	HMI
1913	0.46 ± 0.27	–	3.28 ± 0.43	–	1.00	5.99 ± 1.24	–
1920	0.33 ± 0.08	–	3.15 ± 0.53	–	1.00	6.14 ± 1.33	–
1930	0.33 ± 0.14	–	3.67 ± 1.02	–	1.00	6.23 ± 2.10	–
1942	0.30 ± 0.15	–	3.19 ± 0.68	–	1.00	5.59 ± 1.71	–
1950	0.21 ± 0.03	–	2.88 ± 0.53	–	1.00	5.45 ± 1.07	–
1961	0.24 ± 0.05	–	2.62 ± 0.21	–	1.00	4.84 ± 0.54	–
1970	0.33 ± 0.06	–	2.89 ± 0.18	–	1.00	4.84 ± 0.43	–
1980	0.28 ± 0.06	–	2.64 ± 0.27	–	1.00	4.77 ± 0.48	–
1990	0.32 ± 0.10	–	2.75 ± 0.23	–	1.00	5.09 ± 0.26	–
2000	0.31 ± 0.05	–	2.87 ± 0.31	–	1.00	5.75 ± 0.92	–
2010	0.32 ± 0.08	–	–	3.06 ± 0.32	1.00	4.99 ± 0.78	–
2017	0.32 ± 0.07	–	–	3.22 ± 0.29	1.00	5.41 ± 0.68	–
2020	0.41 ± 0.14	–	–	3.16 ± 0.37	1.00	5.16 ± 0.91	–
2030	0.28 ± 0.14	–	–	3.16 ± 0.37	1.00	5.68 ± 0.91	–
2047	0.36 ± 0.13	1.79 ± 0.28	–	3.77 ± 0.30	1.00	5.57 ± 0.76	–
2049	0.34 ± 0.13	2.06 ± 0.54	–	3.74 ± 0.46	1.00	6.67 ± 0.86	–
2052	0.31 ± 0.17	1.85 ± 0.30	–	3.56 ± 0.34	1.00	6.93 ± 1.91	–
2060	0.31 ± 0.15	1.52 ± 0.18	–	3.59 ± 0.26	1.00	6.44 ± 1.02	–
2068	0.25 ± 0.13	1.87 ± 0.20	–	3.48 ± 0.35	1.00	6.89 ± 1.58	–
2070	0.24 ± 0.07	1.73 ± 0.15	–	3.71 ± 0.38	1.00	6.94 ± 1.24	–
2071	0.29 ± 0.09	1.82 ± 0.11	–	3.75 ± 0.24	1.00	7.74 ± 0.96	–
2080	0.18 ± 0.03	1.53 ± 0.21	–	3.26 ± 0.36	1.00	6.95 ± 0.69	–
2088	0.21 ± 0.05	1.44 ± 0.12	–	3.13 ± 0.53	1.00	6.45 ± 1.52	–
2097	0.36 ± 0.11	1.89 ± 0.33	–	2.76 ± 0.34	1.00	5.92 ± 1.36	5.49 ± 1.38
2104	0.26 ± 0.08	–	–	2.13 ± 0.27	1.00	4.50 ± 0.92	3.89 ± 0.92
2110	0.37 ± 0.14	–	–	2.80 ± 0.30	1.00	–	4.73 ± 1.10
2114	0.37 ± 0.14	–	–	2.39 ± 0.38	1.00	–	4.73 ± 1.10
2117	0.35 ± 0.11	–	–	2.54 ± 0.16	1.00	–	3.80 ± 0.73
2119	0.33 ± 0.19	–	–	2.34 ± 0.31	1.00	–	3.78 ± 0.92
2123	0.35 ± 0.19	–	–	2.59 ± 0.18	1.00	–	4.16 ± 0.85
2126	0.35 ± 0.14	–	–	2.52 ± 0.30	1.00	–	3.88 ± 0.88

7. Summary and Discussion

In this report, we have compared synoptic maps from seven observatories in an effort to find a "ground truth" estimate for the photospheric magnetic field. We found that the maps generally agree with one another but that there are some significant quantitative differences. We provided several tables of conversion factors so that data from one observatory can be converted to data that would match measurements made at another observatory, but temporal variations over a solar cycle suggest that care must be taken in how they are used.

The differences we found between the synoptic maps can substantially affect the global PFSS and MHD models, particularly in the computation of the open, unsigned heliospheric flux. Consider a PFSS solution, for example. Since the magnetic field is potential, solutions are found by solving Laplace's equation: $\nabla^2 \chi = 0$, where χ is a scalar potential. In the simplest application of this model, the only free parameter is the radius of the source surface, that is, the distance from the Sun where all field lines are required to become radial. This is typically taken to be $2.5R_S$. What this means is that multiplication of the photospheric magnetic field boundary condition by some constant factor results in the open flux that passes through the source surface increasing by that same amount. Alternatively, the amount of open flux can be modulated by moving the source surface in (out) and increasing (decreasing) the amount of open flux. Although the situation is more complicated with MHD models because of the relative strengths of plasma and magnetic field pressures, similar effects are found (Stevens *et al.*, 2012). Thus, given the free parameters in the model, it should be possible to take any input synoptic map and make the open flux agree with *in-situ* measurements. In fact, there seems to be a notable deficit. That is, MHD models predict field strengths that are substantially ($2 - 3$ times) lower than are observed at 1 AU (Riley *et al.*, 2012). This may be the result of using photospheric field strengths that are too low, or from a new idea, that a significant amount of unipolar flux is present (but not well observed) near the poles of the Sun (Linker *et al.*, 2012).

There are many possible sources of the differences we see from one synoptic map to another. First, for ground-based instruments, seeing caused by atmospheric turbulence can effectively blur the resulting image. Similarly, telescope jitters, which could result from a number of sources, including tracking problems, stability of the telescope, and temperature variations, can reduce the effective resolution of the instrument. Second, incorrect calibration of the polarization modulation, leading to potentially nonlinear errors in the conversion of instrument units to real units. Third, the choice in the spectral line could lead to intrinsic differences between the maps. As is well known, different spectrum lines may be formed at different heights in the expanding magnetic flux of network features, thus, different lines may not measure the same magnetic fields. Fourth, the algorithms used to convert the raw data measured by the instruments could contain errors. In the specific case of synoptic maps, this is additionally complicated by the extra steps in converting the disk magnetograms to Carrington maps and conserving flux in this transformation. Fifth, we must recognize that for these line-of-sight measurements, an average of the magnetic field strength over a particular area is not the same as the average of a line shift over that area, which is then converted into field strength. Thus, our assumption that we can degrade the spatial resolution of a more highly-resolved map to that of a lower-resolution map by simple averaging is strictly not true. Sixth, the line-of-sight component of the photospheric field includes an increasing contribution from poorly resolved, but rapidly changing horizontal fields as one approaches the limb (including the poles). This should not be treated as a radial field, but in practice often is. And, while it is difficult to assess its impact, to the extent that it does not average to zero within a particular pixel, it may be a source of discrepancy between different datasets.

An additional and distinct set of problems arises from instrumental effects, which can appear at different observatories, at different times, and for both known and (at least initially) unknown reasons. Several examples serve to illustrate this problem. First, toward the end of the MDI mission, the zero-level drifted. Second, there is a known scaling problem with GONG in the sense that it measures signals that are approximately 70 % of what they should be. The reason is not clear: The field measurement is simply the difference between the Doppler-shift images made in left- and right-circularly polarized light. The velocities are what one anticipates from solar rotation and the circular polarization modulation has

been measured to be essentially 100 % efficient. Third, the modulator in the SOLIS instrument slowly degraded from 2003 to 2006, resulting in weaker signals. This was corrected in March 2006, resulting in higher signals. Fourth, the cameras in the SOLIS instrument were replaced in late 2009, resulting in another jump in the signal. These effects are not immediately evident in the analysis presented here. And fifth, and again concerning SOLIS, the current modulator has a spatial variation across the disk such that the signals from the west limb are weaker than those from the east limb. This effect is corrected for by a calibrating function, but it is not known how stable the phenomenon is.

This study did not resolve the illusive problem of finding an underlying "ground truth" for the photospheric magnetic field. It might have been tempting to infer from the seamless continuity between KPVT/SOLIS and MDI/HMI pairs that one of these might have provided the most accurate estimate of the photospheric field. However, these continuities were accomplished by design and are not the result of independence. MDI and SOLIS, at least using synoptic map pixel-by-pixel comparisons, resulted in conversion factors that were very close to one. Since the instruments/observatories are managed independently by different teams at different locations, does this provide any evidence for a "ground truth?" Unfortunately, and again, the data-processing pipelines are not strictly independent. Liu *et al.* (2012) described that they used a previous analysis by Tran *et al.* (2005), which compared MDI and MWO magnetograms to bring the MDI measurements into agreement with MWO values. While the logic behind the application of the MWO correction factor appears to be theoretically justified, such bootstrapping prevents us from inferring this as evidence of a "ground truth."

Another limitation of the present study, and one of our own making, is the use of synoptic maps instead of magnetograms. Our rationale for this was that these maps are used to drive global numerical models and thus represent a practical starting point for the comparison. However, significant processing has occurred between magnetograms and maps. The relationship between a resolution element in the synoptic map and the original magnetogram, in particular, is quite remote. At WSO, for example, the native pixel size is 3 arcmin. The raw magnetograms are composed of 11 scan lines in latitude and 23 positions in longitude; the apertures in the longitude direction overlapping by 50 %. These are then remapped into heliographic coordinates and interpolated using a polynomial smoothing function, which produces a regular map with 5-degree steps in Carrington longitude and 30 points in sin-latitude. These magnetograms are then used to construct the synoptic maps, which involves using all observations of a given point within 55° of central meridian to construct an average value. No adjustment for any radial projection is made in this process. Ultimately, it may be that no "ground truth" can be found from an analysis of the synoptic maps: Instead, we must directly compare the disk magnetograms.

There are at least several avenues we could pursue to resolve some of the issues raised here. First, we could compare our conversion factors with those obtained by looking at the mean magnetic field of the Sun (MMFS), that is, the strength of the line-of-sight component of the photospheric field averaged over the entire visible hemisphere (Scherrer *et al.*, 1977). However, it is not clear whether the factors obtained from such a comparison would be expected to match those obtained here. In fact, MMFS comparisons between SOLIS and HMI produce substantially different results than resolved-image comparisons (Pietarila *et al.*, 2013). Second, we could analyze the disk magnetograms directly. This would allow us to at least separate out intrinsic differences between the measurements and differences introduced through the process of assembling the maps. Three preliminary but independent studies by co-authors of this paper, however, do not appear to be converging on a consensus view. It appears that the results are sensitive to one of a number of potential effects: i) How

the data are binned, ii) which intervals are chosen, and iii) what fitting techniques are applied to the scatterplots. We are currently designing more focused investigations to remove these contaminations, or at least assess their effects on the results.

In closing, we reiterate that the main point of this study was to quantitatively assess the differences between synoptic magnetograms from a selection of solar observatories, and if possible, identify a "ground truth" dataset. While successful on the former, we were not able to find evidence to support using one dataset over another. PFSS and MHD numerical models may be able to help us resolve this; however, the presence of free parameters within the model will make such a study challenging. On the other hand, the unique nature of the recent protracted solar minimum may provide the necessary conditions to accurately connect the magnetic flux observed *in situ* at 1 AU with that observed in the photosphere through a global model, if used in conjunction with other observed constraints, such as the measured bulk solar wind speed, location of coronal hole boundaries, and disk emission profiles.

References

Arge, C.N., Henney, C.J., Koller, J., Compeau, C.R., Young, S., MacKenzie, D., Fay, A., Harvey, J.W.: 2010, Air Force data assimilative photospheric flux transport (ADAPT) model. In: Maksimovic, M., Issautier, K., Meyer-Vernet, N., Moncuquet, M., Pantellini, F. (eds.) *Twelfth International Solar Wind Conference*, *AIP Conf. Proc.* **1216**, 343 – 346. doi:10.1063/1.3395870.

Berger, T.E., Lites, B.W.: 2002, Weak-field magnetogram calibration using advanced Stokes polarimeter flux-density maps – I. Solar optical universal polarimeter calibration. *Solar Phys.* **208**, 181 – 210. doi:10.1023/A:1020537923728.

Bering, E.A., Benbrook, J.R., Engebretson, M.J., Arnoldy, R.L.: 1998, Simultaneous electric and magnetic field observations of Pc1 – 2, and Pc3 pulsations. *J. Geophys. Res.* **103**, 6741 – 6762. doi:10.1029/97JA03327.

Bertello, L., Petrie, G.J., Tran, T.: 2010, The impact of different global photospheric magnetic field maps on coronal models. In: AGU Fall Meeting, SH31B-1796.

Cauzzi, G., Smaldone, L.A., Balasubramaniam, K.S., Keil, S.L.: 1993, On the calibration of line-of-sight magnetograms. *Solar Phys.* **146**, 207 – 227. doi:10.1007/BF00662010.

Demidov, M.L., Balthasar, H.: 2009, Spectro-polarimetric observations of solar magnetic fields and the SOHO/MDI calibration issue. *Solar Phys.* **260**, 261 – 270. doi:10.1007/s11207-009-9443-5.

Demidov, M.L., Balthasar, H.: 2012, On multi-line spectro-polarimetric diagnostics of the quiet Sun's magnetic fields. Statistics, inversion results and effects on the SOHO/MDI magnetogram calibration. *Solar Phys.* **276**, 43 – 59. doi:10.1007/s11207-011-9863-x.

Demidov, M.L., Golubeva, E.M., Balthasar, H., Staude, J., Grigoryev, V.M.: 2008, Comparison of solar magnetic fields measured at different observatories: peculiar strength ratio distributions across the disk. *Solar Phys.* **250**, 279 – 301. doi:10.1007/s11207-008-9225-5.

Jones, H.P.: 1989, Magnetograph group summary. In: Winglee, R.M., Dennis, B.R. (eds.) *Max'91 Workshop2: Developments in Observations and Theory for Solar Cycle 22*, NASA-TM-101893, 17 – 26.

Jones, H.P.: 1992a, Calibrating the NASA/NSO spectromagnetograph. *Bull. Am. Astron. Soc.* **24**, 814.

Jones, H.P.: 1992b, Comparison of magnetograms by histogram equating. *Bull. Am. Astron. Soc.* **24**, 1252.

Jones, H.P., Ceja, J.A.: 2001, Preliminary comparison of magnetograms from KPVT/SPM, SOHO/MDI and GONG$^+$. In: Sigwarth, M. (ed.) *Advanced Solar Polarimetry – Theory, Observation, and Instrumentation*, *ASP Conf. Ser.* **236**, 87 – 95.

Jones, H.P., Duvall, T.L. Jr., Harvey, J.W., Mahaffey, C.T., Schwitters, J.D., Simmons, J.E.: 1992, The NASA/NSO spectromagnetograph. *Solar Phys.* **139**, 211 – 232. doi:10.1007/BF00159149.

Jones, H., Bogart, R., Canfield, R., Chapman, G., Henney, C., Kopp, G., *et al.*: 1993, A magnetograph comparison workshop. *Bull. Am. Astron. Soc.* **25**, 1216.

Jones, H.P., Harvey, J.W., Henney, C.J., Keller, C.U., Malanushenko, O.M.: 2004, Measurement scale of the SOLIS vector spectromagnetograph. *Bull. Am. Astron. Soc.* **36**, 709.

Landi Degl'Innocenti, E.: 1982, On the effective Lande factor of magnetic lines. *Solar Phys.* **77**, 285. doi:10.1007/BF00156111.

Linker, J.A., Mikic, Z., Riley, P., Downs, C., Lionello, R., Henney, C., Arge, C.N.: 2012, Coronal and heliospheric modeling using flux-evolved maps. In: *Proceedings of Solar Wind 13*, *AIP Conf. Proc.* **1539**, 26 – 29.

Liu, Y., Hoeksema, J.T., Scherrer, P.H., Schou, J., Couvidat, S., Bush, R.I., Duvall, T.L., Hayashi, K., Sun, X., Zhao, X.: 2012, Comparison of line-of-sight magnetograms taken by the Solar Dynamics Observatory/Helioseismic and Magnetic Imager and Solar and Heliospheric Observatory/Michelson Doppler Imager. *Solar Phys.* **279**, 295 – 316. doi:10.1007/s11207-012-9976-x.

Lockwood, M.: 2001, Long-term variations in the magnetic fields of the Sun and the heliosphere: their origin, effects, and implications. *J. Geophys. Res.* **106**, 16021 – 16038. doi:10.1029/2000JA000115.

Lockwood, M., Owens, M.J.: 2011, Centennial changes in the heliospheric magnetic field and open solar flux: the consensus view from geomagnetic data and cosmogenic isotopes and its implications. *J. Geophys. Res.* **116**, 4109. doi:10.1029/2010JA016220.

Lockwood, M., Stamper, R., Wild, M.N.: 1999, A doubling of the Sun's coronal magnetic field during the past 100 years. *Nature* **399**, 437 – 439.

Luhmann, J., Lee, C.O., Riley, P., Jian, L.K., Russell, C.T., Petrie, G.: 2012, Interplanetary conditions: lessons from this minimum. In: Mandrini, C.H., Webb, D.F. (eds.) *Comparative Magnetic Minima: Characterizing Quiet Times in the Sun and Stars*, *IAU Symp.* **286**, 168 – 178. doi:10.1017/S1743921312004802.

Petrie, G.J.D., Canou, A., Amari, T.: 2011, Nonlinear force-free and potential-field models of active-region and global coronal fields during the whole heliosphere interval. *Solar Phys.* **274**, 163 – 194. doi:10.1007/s11207-010-9687-0.

Pietarila, A., Bertello, L., Harvey, J.W., Pevtsov, A.A.: 2013, Comparison of ground-based and space-based longitudinal magnetograms. *Solar Phys.* **282**, 91 – 106. doi:10.1007/s11207-012-0138-y.

Riley, P.: 2007, An alternative interpretation of the relationship between the inferred open solar flux and the interplanetary magnetic field. *Astrophys. J. Lett.* **667**, L97 – L100. doi:10.1086/522001.

Riley, P., Lionello, R., Linker, J.A., Mikic, Z., Luhmann, J., Wijaya, J.: 2011, Global MHD modeling of the solar corona and inner heliosphere for the whole heliosphere interval. *Solar Phys.* **274**, 361 – 375. doi:10.1007/s11207-010-9698-x.

Riley, P., Linker, J.A., Lionello, R., Mikic, Z.: 2012, Corotating interaction regions during the recent solar minimum: the power and limitations of global MHD modeling. *J. Atmos. Solar-Terr. Phys.* **83**, 1 – 10. doi:10.1016/j.jastp.2011.12.013.

Scherrer, P.H., Wilcox, J.M., Svalgaard, L., Duvall, T.L. Jr., Dittmer, P.H., Gustafson, E.K.: 1977, The mean magnetic field of the Sun – observations at Stanford. *Solar Phys.* **54**, 353 – 361. doi:10.1007/BF00159925.

Scherrer, P.H., Bogart, R.S., Bush, R.I., Hoeksema, J.T., Kosovichev, A.G., Schou, J., *et al.*: 1995, The Solar Oscillations Investigation – Michelson Doppler Imager. *Solar Phys.* **162**, 129 – 188. doi:10.1007/BF00733429.

Stellman, J.: 1998, *Encyclopaedia of Occupational Health and Safety*, International Labour Office, Geneva.

Stevens, M.L., Linker, J.A., Riley, P., Hughes, W.J.: 2012, Underestimates of magnetic flux in coupled MHD model solar wind solutions. *J. Atmos. Solar-Terr. Phys.* **83**, 22 – 31. doi:10.1016/j.jastp.2012.02.005.

Svalgaard, L.: 2006, How good (or bad) are the inner boundary conditions for heliospheric solar wind modeling? Presentation at 2006 SHINE Workshop.

Svalgaard, L., Cliver, E.W.: 2005, The IDV index: Its derivation and use in inferring long-term variations of the interplanetary magnetic field strength. *J. Geophys. Res.* **110**, A12103. doi:10.1029/2005JA011203.

Svalgaard, L., Duvall, T.L. Jr., Scherrer, P.H.: 1978, The strength of the Sun's polar fields. *Solar Phys.* **58**, 225 – 239. doi:10.1007/BF00157268.

Thornton, C.E., Jones, H.P.: 2002, Comparison of three solar magnetographs. *Bull. Am. Astron. Soc.* **34**, 1243.

Tran, T., Bertello, L., Ulrich, R.K., Evans, S.: 2005, Magnetic fields from SOHO MDI converted to the Mount Wilson 150 foot Solar Tower scale. *Astrophys. J. Suppl.* **156**, 295 – 310. doi:10.1086/426713.

Ulrich, R.K.: 1992, Analysis of magnetic fluxtubes on the solar surface from observations at Mt. Wilson of λ5250 and λ5233. In: Giampapa, M.S., Bookbinder, J.A. (eds.) *Seventh Cambridge Workshop: Cool Stars, Stellar Systems, and the Sun*, *ASP Conf. Ser.* **26**, 265 – 267.

Ulrich, R.K., Bertello, L., Boyden, J.E., Webster, L.: 2009, Interpretation of solar magnetic field strength observations. *Solar Phys.* **255**, 53 – 78. doi:10.1007/s11207-008-9302-9.

Wang, Y.M., Sheeley, N.R.: 1995, Solar implications of Ulysses interplanetary field measurements. *Astrophys. J. Lett.* **447**, L143 – L146. doi:10.1086/309578.

Wenzler, T., Solanki, S.K., Krivova, N.A., Fröhlich, C.: 2006, Reconstruction of solar irradiance variations in cycles 21 – 23 based on surface magnetic fields. *Astron. Astrophys.* **460**, 583 – 595. doi:10.1051/0004-6361:20065752.